

Compact dual-band filtering power divider with independently controllable bandwidths using shorted patch resonators

ISSN 1751-8725
 Received on 22nd October 2019
 Revised 8th January 2020
 Accepted on 11th March 2020
 E-First on 23rd April 2020
 doi: 10.1049/iet-map.2019.0916
 www.ietdl.org

Gaoya Dong¹, Weimin Wang¹, Yongle Wu¹ ✉, Yuanan Liu¹, Yunnan Fang², Manos M. Tentzeris²

¹Beijing Key Laboratory of Work Safety Intelligent Monitoring, School of Electronic Engineering, Beijing University of Posts and Telecommunications, P.O. Box 282, Beijing 100876, People's Republic of China

²School of Electrical Computer Engineering, Georgia Institute of Technology, Atlanta, GA 30332, USA

✉ E-mail: wuyongle138@gmail.com

Abstract: This study presents a novel dual-band filtering power divider (DB-FPD) structure with independently controllable bandwidths for dual-band application. The proposed DB-FPD structure is constructed by shorted G- and T-shaped patch resonators, and meandered slot lines are etched on shorted patch resonators to generate resonance in the upper band. The 3 dB fractional bandwidth (FBW) of designed DB-FPD structure in a lower band (upper band) can be adjusted from 5.2 to 24.2% (3.1 to 26.9%), respectively, using a substrate of 31 mil thick TLY-5. The even-/odd-mode method is adopted to demonstrate the power splitting and isolation performances. The lumped-element equivalent circuit is extracted to explain the power splitting transmission performance. Also, the coupling matrix analysis is applied to present the detailed design procedures for practical DB-FPD, with specific passband bandwidths and centre frequencies of dual passbands. Finally, the isolation performances are analysed with different isolation resistor values and loading positions. For verification, two DB-FPDs with equal absolute bandwidths (ABW) and equal FBWs are simulated, fabricated and measured for dual-band WLAN application. The measured results agree well with the simulated ones, exhibiting a favourable frequency selectivity and controllable passband bandwidths.

1 Introduction

Power dividers (PDs) and bandpass filters (BPFs) are widely used in modern wireless communication systems. To obtain the reduced size and low insertion loss, filtering PD (FPD) is proposed, which can provide both functions of frequency selection and power splitting/combining. One common method to design FPDs is to cascade the filtering structures with conventional PDs [1–3]. However, the sizes of circuits still occupy large spaces by adopting this method. Compact in-phase PD integrated filtering response is presented in [4] by utilising spiral resonators. Based on composite right/left-handed transmission lines (TLs), a compact three-way FPD is introduced in [5]. The FPDs presented in [1–5] are all operating at a single band.

With the development of multi-band and multi-standard modern wireless communication systems, the multi-band microwave components are in great demand. Some efforts [6–13] have been made to design dual-band filtering power dividers (DB-FPDs). In [6], a DB-FPD is designed by replacing the conventional quarter-wavelength TLs with BPFs, and the isolation elements are loaded at the open ends of filter to realise good isolation between the output ports. However, the circuit presented in [6] occupies a large size. Compact DB-FPDs are introduced in [7–13] by adopting various methods. Based on the traditional Wilkinson PD, a compact DB-FPD is presented in [7] by employing T-junction structures and quarter-wavelength stepped impedance resonators. A novel DB-FPD is proposed in [8] by adopting two coupled ring resonators. In [9], a compact DB-FPD with capacitor-loaded centrally coupled-line resonators is presented. The integrated stub-loaded resonators are applied in [10–12] to design PDs with dual-band filtering response and compact size. By introducing a proper coupling topology between the quarter-wavelength short-ended microstrip line and two multi-mode resonators, a DB-FPD is introduced in [13]. The passband bandwidths in the lower band and upper band of DB-FPDs proposed in [6–13] cannot be independently controlled. A DB-FPD with independently controllable bandwidth (ICBW) is designed in [14] based on short- and open-circuited stubs. However, the DB-FPD presented in [14]

occupies a large space. Thus, the DB-FPDs with ICBW and compact size are demanded.

The DB-FPD with ICBW and compact size is proposed in this paper based on shorted patch resonators, and meandered slot lines (MSLs) are etched on shorted patch resonators to introduce resonance in the upper band. The passband bandwidths in the lower band and the upper band can be independently adjusted by tuning the dimensions of MSLs, locations of feeding points as well as the gaps between shorted patch resonators. The even-/odd-mode method is applied to analyse the transmission and isolation performances. The coupling matrix analysis is applied to design DB-FPD with specific passband bandwidths and centre frequencies. Two prototype DB-FPDs with equal fractional bandwidth (FBW) and equal absolute bandwidths (ABW) are fabricated on the substrate with a dielectric of 2.55 and a thickness of 31 mil to verify the proposed design concept. Both simulated and measured results are in good agreement, exhibiting a favourable frequency selectivity and independently controllable passband bandwidths.

2 Analysis and design

2.1 Layout of proposed DB-FPD

The presented dual-band FPD structure is sketched in Fig. 1a, and the characteristic impedances of the input port and output ports are all selected as 50Ω . The FPD structure shown in Fig. 1a is composed of four shorted G-shaped patch resonators, two shorted T-shaped patch resonators and three isolation resistors (R_1 , R_2 and R_3). Moreover, MSLs are etched on shorted patch resonators to introduce resonances in the upper band, as shown in Fig. 2, and isolation resistors are adopted to improve the isolation level between ports 2 and 3. As the designed FPD structure is symmetrical, the even- and odd-mode equivalent circuits of presented DB-FPD are shown Figs. 1b and c, respectively. The equivalent circuit of designed DB-FPD can be considered as a BPF where ports 1 and 2 are selected as 100 and 50Ω , respectively. Based on the lumped-element equivalent circuit exhibited in Fig. 3, the resonance frequency in the lower band produced by G- and T-

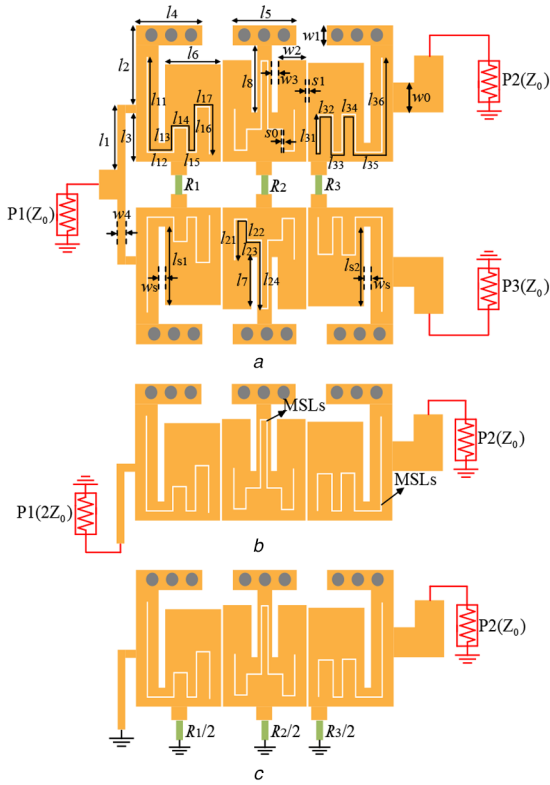


Fig. 1 The configuration of (a) proposed DB-FPD, (b) Even, (c) Odd-mode equivalent circuit

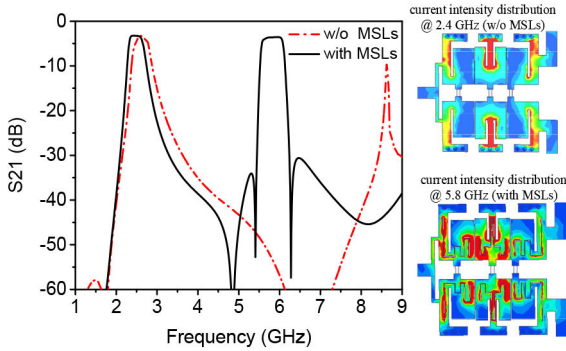


Fig. 2 Transmission performances and current distributions of presented DB-FPD with or without MSLs

shaped shorted patch resonators can be expressed as (1a). According to Fig. 1a, the MSLs are acting as quarter-wavelength resonators, thus the resonance frequency in the upper band can be deduced as (1b) by setting $l_{x1} = l_{11} + l_{12} + l_{13} \times 2 + l_{14} + l_{15} + l_{16} \times 2 + l_{17}$, $l_{x2} = 2 \times (l_{21} + l_{22} + l_{23} + l_{24})$ and $l_{x1} = l_{x2}$:

$$f_{G,T}^I = \frac{1}{2\pi\sqrt{(L_g^I + L_p^I)C_p^I}} \quad (1a)$$

$$f_G^II = \frac{1}{2l_{x1}\sqrt{\epsilon_{eff}}}, \quad f_T^II = \frac{1}{2l_{x2}\sqrt{\epsilon_{eff}}} \quad (1b)$$

2.2 Analysis of transmission performance

To analyse the influence of MSLs, the transmission coefficients of DB-FPD with or without MSLs are plotted in Fig. 2. Moreover, the current intensity distributions operating at 2.4 and 5.8 GHz are also exhibited. It can be seen from Fig. 2 that resonance centred at 2.4 GHz is mainly realised by employing shorted G- and T-shaped patch resonators, and resonance centred at 5.8 GHz is introduced by etching MSLs.

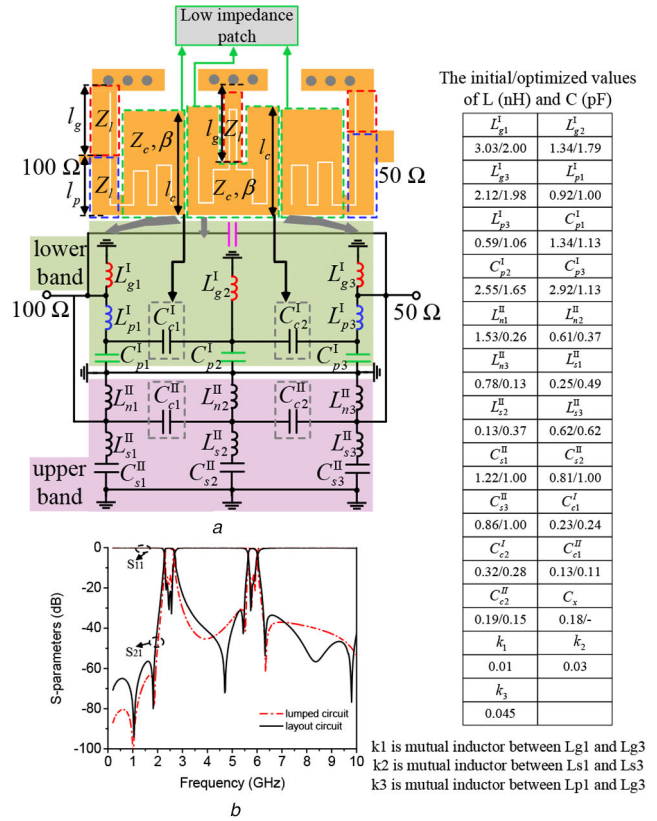


Fig. 3 The equivalent lumped-element circuit model and frequency response

(a) Equivalent lumped-element circuit model of even-mode schematic, (b) Frequency response comparisons of lumped-element circuit and EM simulation

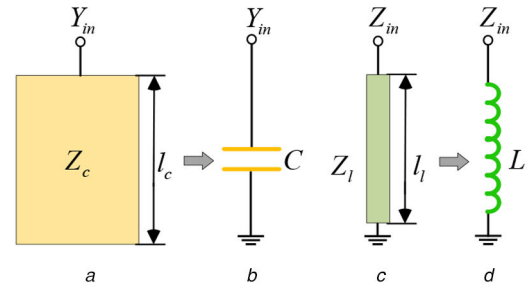


Fig. 4 The Short stub elements

(a) Open-circuited stub, (b) Equivalent capacitor, (c) Short-circuited stub, (d) Equivalent inductor

The equivalent lumped-element circuit model of the even-mode equivalent circuit shown in Fig. 1b can be extracted in Fig. 3a. In G- and T-shaped resonators, the TL between shorting vias and loading point can be modelled as L_g^I , and the TL connecting loading point and patch is modelled as L_p^I . The low impedance patch can be modelled as C_p^I . Based on [15], the open-circuited stub of lossless microstrip line can be equivalent to a shunt capacitor and that a similar short-circuited stub could be equivalent to a shunt inductor, as indicated in Fig. 4. Based on the TL theory, the input admittance (impedance) of open- (short-)circuited TL can be expressed as eq. (2a) and (2b). When $l_0 < \lambda_g/8$, the input admittance (impedance) could be approximated as eq. (3a) and (3b). Thus, the values of L_g^I , L_p^I and C_p^I can be deduced as eq. (4a), (4b) and (4c) based on (2) and (3), where Z_l as well as l_p (l_g) represent the characteristic impedance and physical length of TL connecting with shorting vias, and Z_c as well as l_c are the characteristics and physical length of low impedance path. The MSLs can be modelled as L_n^II , L_s^II and C_s^II . Assume C_s^II is 1 pF, the values of L_n^II , L_s^II can be deduced as (5a) based on [15], where ω , Q and G represent the operating frequency, external quality factor and

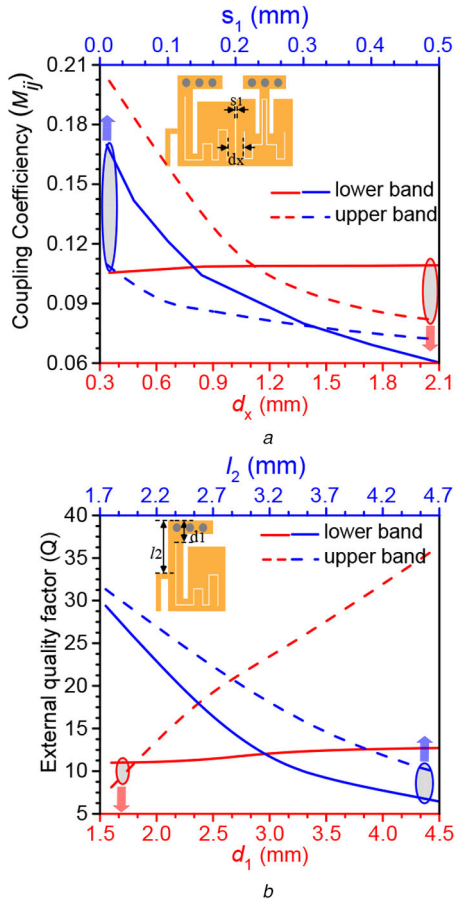


Fig. 5 The coupling coefficient and external quality factor with various parameter values
 (a) M^I and M^{II} with varied d_x ($s_1 = 0.15$ mm) and s_1 ($d_x = 0.1$ mm), (b) Q^I and Q^{II} with varied l_2 ($d_1 = 2.35$ mm) and d_1 ($l_2 = 3.0$ mm)

input port admittance. C_c^I is used to model the coupling between shorted G- and T-shaped patch resonators, while C_c^{II} is used to model the coupling between MSLs. Thus, the initial values of inductors and capacitors can be calculated from (4a), (4b), (4c), (5a), (5b) and (5c). The frequencies of transmission zeros (TZs) can be adjusted by tuning the values of C_x , k_1 , k_2 and k_3 . Then the values of inductors and capacitors are optimised to fit EM simulation results, exhibited in Fig. 3. Accordingly, the frequency responses of the lumped-element circuit and EM simulation agree well. As observed from the initial values and optimised values exhibited in Fig. 3, eq. (4a), (4b), (4c), (5a), (5b) and (5c) can provide effective guidance for selecting the values of capacitance and inductance in equivalent lumped-element circuit model of the even-mode schematic:

$$Y_{in} = jY_c \cdot \tan(2\pi \cdot l_c / \lambda_g) \quad (2a)$$

$$Z_{in} = jZ_l \cdot \tan(2\pi \cdot l_l / \lambda_g) \quad (2b)$$

$$Y_{in} \approx jY_c \cdot (2\pi \cdot l_c / \lambda_g) = j\omega C \quad (3a)$$

$$Z_{in} \approx jZ_l \tan(2\pi \cdot l_l / \lambda_g) = j\omega L \quad (3b)$$

$$C_p^I = (2\pi \cdot l_c) / (Z_c \cdot \lambda_g \cdot \omega) \quad (4a)$$

$$L_p^I = (2\pi \cdot Z_l \cdot l_p) / (\lambda_g \cdot \omega) \quad (4b)$$

$$L_g^I = (2\pi \cdot Z_l \cdot l_g) / (\lambda_g \cdot \omega) \quad (4c)$$

$$L_n^{II} = 1/\omega \cdot Q \cdot G, \quad L_s^{II} = 1/\omega^2 \cdot C_s - 1/\omega \cdot Q \cdot G \quad (5a)$$

$$C_c^I = M_{ij} \cdot C_{eq}^I, \quad C_{eq}^I = C_p^I / (1 - \omega^2 \cdot C_p^I \cdot L_p^I) \quad (5b)$$

$$C_c^{II} = M_{ij} \cdot C_{eq}^{II}, \quad C_{eq}^{II} = C_p^{II} / (1 - \omega^2 \cdot C_p^{II} \cdot L_p^{II}) \quad (5c)$$

According to [15], in order to design a three-order Chebyshev filter when the input impedance and output characteristic impedance are all selected as 50Ω , the coupling coefficient ($M'_{i,i+1}$) and external quality factor (Q'_{ei} , Q'_{eo}) should satisfy (6). The circuit elements of the low-pass prototype filter with 0.1 dB ripple level are found to be $g_0 = 1$, $g_1 = 1.0316$, $g_2 = 1.1474$, $g_3 = 1.0316$ and $g_4 = 1.0$:

$$M'_{i,i+1} = \frac{FBW}{\sqrt{g_i g_{i+1}}} \quad (i \in 1, 2, \dots, n-1), \quad Q'_{ei} = Q'_{eo} = \frac{g_0 g_1}{FBW} \quad (6)$$

Specifically, in the even-mode equivalent circuit of designed DB-FPD, i.e. the power splitting equivalent circuit, the impedances of ports 1 and 2 are 100 and 50Ω , respectively. According to [15], the coupling coefficients between shorted patch resonators (M_{12} , M_{23}) and external quality factors (Q_{ei} , Q_{eo}) should meet eq. (7a) and (7b) to obtain good transmission performance under the even-mode excitation:

$$M_{12} = M'_{12}/2, \quad Q_{ei} = Q'_{ei} \cdot \sqrt{2} \quad (7a)$$

$$M_{23} = M'_{23}, \quad Q_{eo} = Q'_{eo} \quad (7b)$$

The coupling coefficients between shorted G- and T-shaped resonators in lower band (M^I) and upper band (M^{II}) with varied d_x and s_1 are depicted in Fig. 5a when employing the substrate presented above. As observed from blue lines in Fig. 5a, when s_1 increases from 0.01 to 0.5 mm, the coupling coefficients in lower band (M^I) and upper band (M^{II}) will rapidly decrease. According to red lines shown in Fig. 5a, when the value of d_x increases from 0.3 to 2.1 mm, the coupling coefficient in lower band (M^I) almost remains constant, and the coupling coefficient in upper band (M^{II}) will decrease. Thus, M^I and M^{II} can be adjusted by tuning the values of s_1 independently, which will help to independently adjust the bandwidths of lower and upper passbands. Radiation is introduced in G- and T-shaped patch resonators by employing MSLs. Thus, the conventional method [15], i.e. extracted by the FBW when the phase ranges from -90° to 90° , cannot be adopted to simulate and calculate the external quality factor of G-shaped resonator. We use the method that constructs a two-order filter by employing two symmetrical G-shaped resonators, then the external quality factor of the G-shaped resonator can be obtained from the simulated FBW and (6). Fig. 5b shows the external quality factors of G-shaped resonator with various d_1 and l_2 when adopting the substrate presented above. It can be concluded from blue lines plotted in Fig. 5b that Q^I in the lower band and Q^{II} in the upper band will decrease when l_2 increases from 1.7 to 4.7 mm. Based on red lines shown in Fig. 5b, when d_1 increases, Q^I in the lower band almost remains constant, while Q^{II} in the upper band increases. Consequently, Q^I and Q^{II} can be adjusted by tuning the value of l_2 . Q^{II} can be further optimised by changing the values of d_1 , while Q^I almost remains constant. Based on the analysis above, M^I , M^{II} , Q^I as well as Q^{II} in presented DB-FPD structure can be adjusted independently, which will help to independently adjust the bandwidths of lower and upper passbands.

In order to verify the proposed method, we extract the external quality factor and coupling matrix for the three-order filter when ports 1 and 2 are selected as 100 and 50Ω , respectively. Moreover, the detailed values are shown in eq. (8a) and (8b). The sign '+' in M_{S1} , M_{12} , M_{23} and M_{3L} represents the magnetic coupling is superior to electric coupling, while the sign '-' in M_{13} and M_{1L} represents the electric coupling is superior to magnetic coupling. TZs can be introduced by adopting mixed electric and magnetic couplings, which is helpful for improving the frequency selectivity.

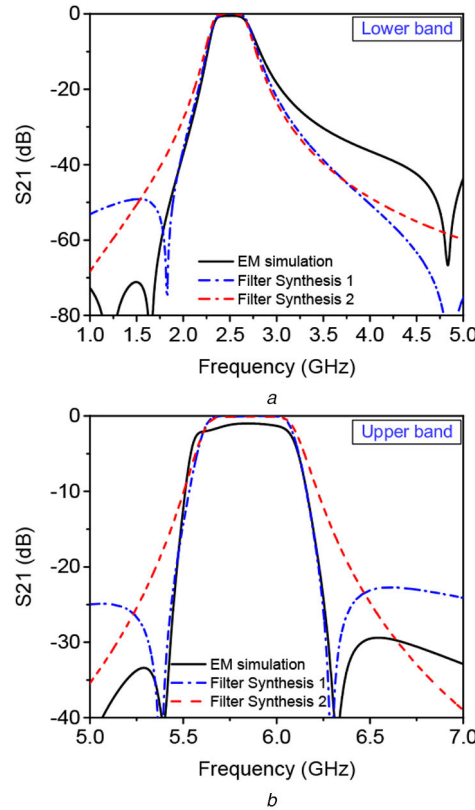


Fig. 6 EM simulation and filter synthesis responses in (a) Lower band, (b) Upper band

Black lines are the EM simulation of even-mode equivalent circuit shown in Fig. 1b, blue lines are filter synthesis 1 based on eq. (8a) and (8b) and red lines are filter synthesis 2 based on eq. (8a) and (8b) when M_{13} and M_{1L} are set to 0

$$\begin{bmatrix} 0 & 0.088 & 0 & 0 & 0 \\ 0.088 & 0 & 0.076 & -0.01 & -0.0016 \\ 0 & 0.076 & 0 & 0.108 & 0 \\ 0 & -0.01 & 0.108 & 0 & 0.125 \\ 0 & -0.0016 & 0 & 0.125 & 0 \end{bmatrix} \quad (8a)$$

$Q_{ei} = 9.40, Q_{eo} = 6.65$ (lower band)

$$\begin{bmatrix} 0 & 0.053 & 0 & 0 & 0 \\ 0.053 & 0 & 0.041 & -0.00039 & -0.014 \\ 0 & 0.041 & 0 & 0.064 & 0 \\ 0 & -0.00039 & 0.064 & 0 & 0.075 \\ 0 & -0.014 & 0 & 0.075 & 0 \end{bmatrix} \quad (8b)$$

$Q_{ei} = 15.00, Q_{eo} = 10.61$ (upper band)

EM simulation for the even-mode equivalent circuit shown in Fig. 1b (black lines), filter synthesis 1 from eq. (8a) and (8b) (blue lines) as well as filter synthesis 1 from eq. (8a) and (8b) when the weak couplings (M_{13} and M_{1L}) are set to be 0 (red lines) are plotted in Fig. 5. As observed in Fig. 5 that EM simulation responses and filter synthesis 1 responses have good agreements in both lower band and upper band. Thus, the coupling matrix theory can help to extract the initial parameters of practical DB-FPD design with specific bandwidths and centre frequencies based on the designed DB-FPD structure. It can be concluded from synthesis 1 and filter synthesis 2 that the passband performance does not change a lot when the weak couplings are set to be 0, and TZs disappear when the weak couplings are set to be 0. Therefore, the passband performance is determined by the strong couplings $M_{S1}, M_{12}, M_{23}, M_{3L}$ and external quality factor Q_{ei}, Q_{eo} . The weak couplings (M_{13} and M_{1L}) have a big influence on stopband performance, i.e. introducing TZs near the passband, which is helpful for improving the frequency selectivity (Fig. 6).

The filter synthesis responses and EM simulation responses of presented DB-FPD with narrowest and widest passband bandwidth based on the employed substrate are shown in Fig. 7. The corresponding values of coupling coefficients as well as external quality factors in various bandwidths are exhibited in Table 1. As observed from Table 1, with a substrate presented above, the centre frequencies in the lower band and the upper band are located at 2.45 and 5.80 GHz, 3 dB FBWs in lower and upper bands range from 5.2 to 24.2% and from 3.1 to 26.9%, respectively. The 3 dB FBWs in the lower band and the upper band are limited by the practical realisable values of coupling coefficients and external quality factor with the adopted substrate, as shown in Fig. 5.

The transmission coefficients of designed DB-FPD adopting various values of s_0 and l_{24} are plotted in Fig. 8. As exhibited, the frequencies of TZs near the upper passband can be adjusted by tuning the values of s_0 and l_{24} . More specifically, f_{TZ1} will shift to the lower band with the bigger value of s_0 , and f_{TZ2} will move to the higher band when the value of s_0 increases. Moreover, the frequencies of f_{TZ1} and f_{TZ2} will shift to the lower band when the length of l_{24} gets longer. The current intensity distribution operating at f_{TZ1} and f_{TZ2} are also exhibited in Fig. 8. Accordingly, TZs can be obtained by selecting the proper dimensions of MSLs.

The return losses of presented DB-FPD with various l_2 and d_x are depicted in Fig. 9. Accordingly, the return losses in the lower band and upper band can be optimised by adjusting the value of l_2 , with nearly constant bandwidths in the lower and upper passbands. By tuning the value of d_x , the return loss in the upper band could be optimised, while the return loss in the lower band almost remains constant. Therefore, by tuning the parameters of l_2 and d_x , good return losses in both lower and upper passbands can be achieved, while the passband bandwidth remains unchanged.

2.3 Analysis of isolation performance

The isolation performances of designed DB-FPD structure with various isolation resistors and different locations are exhibited in

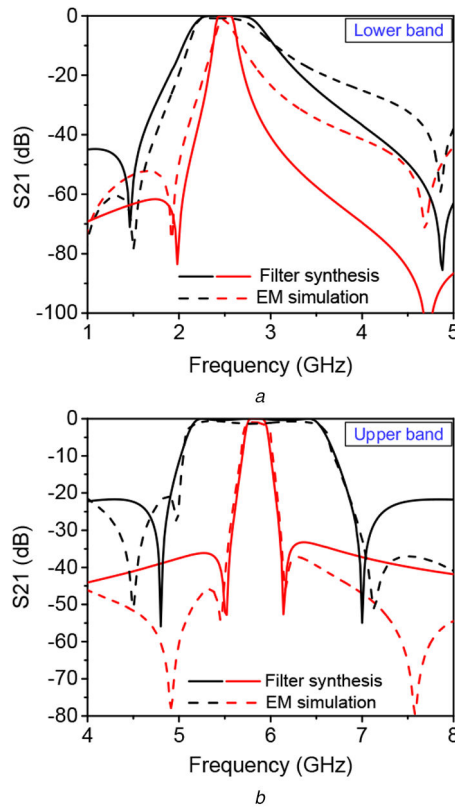


Fig. 7 Transmission performance of designed DB-FPD with narrowest and widest passband bandwidths in (a) Lower band, (b) Upper band

Table 1 Specific coupling coefficient and external quality factor of proposed DB-FPD-1 (DB-FPD2)

	$M_{S1}(M_{1S})$	$M_{12}(M_{21})$	$M_{23}(M_{32})$	$M_{3L}(M_{L3})$	$M_{13}(M_{31})$	$M_{1L}(M_{L1})$	Q_{ci}	Q_{co}
lower band, FBW (5.2%)	0.040	0.038	0.054	0.056	-0.004	-0.0003	23.16	16.38
lower band, FBW (24.2%)	0.18	0.14	0.20	0.26	-0.009	-0.007	4.99	3.53
upper band, FBW (3.1%)	0.023	0.020	0.028	0.033	0.0015	-0.002	39.40	27.86
upper band, FBW (26.9%)	0.137	0.103	0.194	0.194	0	-0.05	10.14	7.17

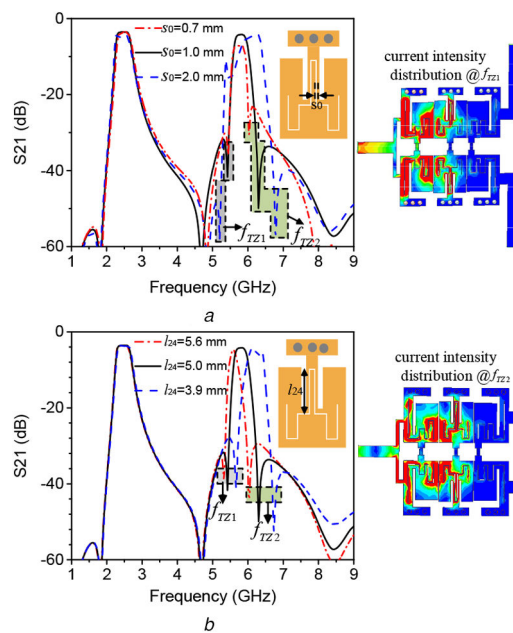


Fig. 8 Transmission performances of presented DB-FPD with various values of (a) s_0 , (b) l_{24}

Fig. 10. It is seen from Fig. 10a that isolation performance in the lower band and the upper band can be adjusted by tuning the values of isolation resistors. According to Fig. 10b, the isolation

performance in the lower band can be further improved by tuning the locations of isolation resistors, while the isolation in the lower band almost remains constant.

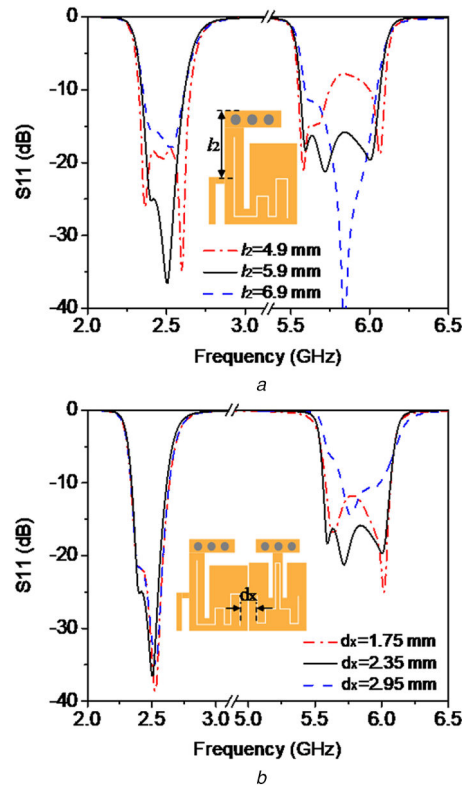


Fig. 9 Return losses of presented DB-FPD with varied (a) l_2 , (b) d_x

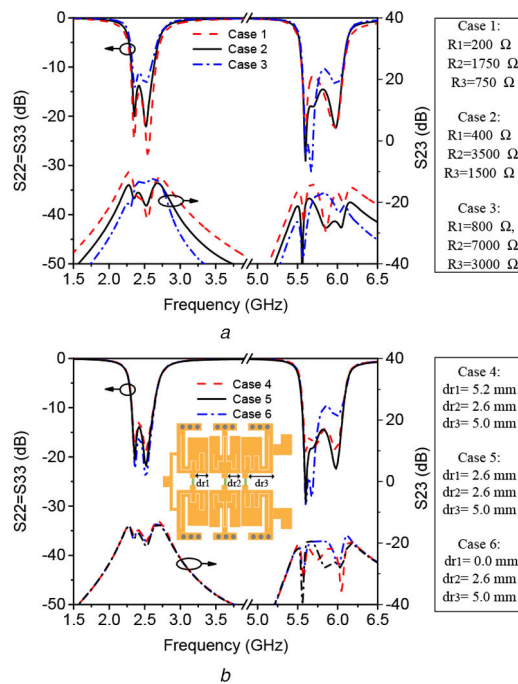


Fig. 10 Isolation performances of presented DB-FPD structure (a) With various isolation resistor values ($d_{r1} = 2.6$ mm, $d_{r2} = 2.6$ mm, $d_{r3} = 5.0$ mm), (b) Resistors located at different locations ($R_1 = 400$ Ω , $R_2 = 3500$ Ω , $R_3 = 1500$ Ω)

2.4 Design procedures

According to the operation principles, centre frequencies and bandwidths adjusting characteristics of lower and upper passbands are analysed in the above sections, the designed procedures of the proposed DB-FPD can be summarised as follows:

- i. Given required f^I and f^{II} , FBWs in the lower band and the upper band, isolation performances.
- ii. Calculate the values of M_{12}^I , M_{23}^I , Q_{ei}^I , Q_{eo}^I , M_{12}^{II} , M_{23}^{II} , Q_{ei}^{II} and Q_{eo}^{II} , based on (6) and eq. (7a) and (7b).
- iii. Deduce the lengths of l_{x1} and l_{x2} , based on (1b).
- iv. Design shorted G- and T-shaped resonators which have resonances at f^I and f^{II} . Optimise the external quality factor of lower bands (Q_{ei}^I , Q_{eo}^I) by tuning the value of l_2 , while the quality factor of the upper bands (Q_{ei}^{II} , Q_{eo}^{II}) can be further adjusted by changing the value of d_1 with almost constants (Q_{ei}^I , Q_{eo}^I), based on Fig. 5b.
- v. Adjust coupling coefficients of lower and upper passbands ((M_{12}^I, M_{23}^I) , $(M_{12}^{II}, M_{23}^{II})$) by changing the value of s_1 . Then,

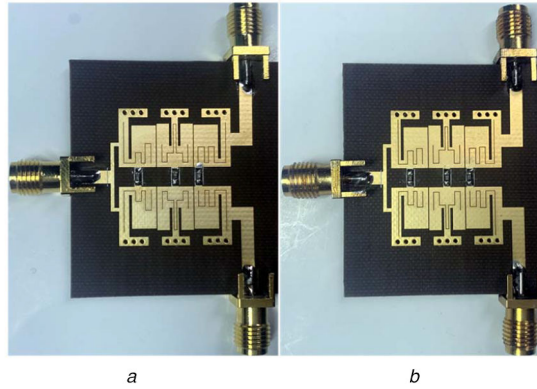


Fig. 11 Photographs of fabricated (a) DB-FPD1, (b) DB-FPD2

Table 2 Specific dimensions of proposed DB-FPD-1 (DB-FPD2) (unit: mm)

w_0	w_1	w_2	w_3	w_4	l_1	l_2	l_3
2.2 (2.2)	1.5 (1.5)	2.1 (2.1)	0.45(0.45)	1.0 (1.0)	4.8 (4.8)	5.9 (5.9)	3.6 (3.6)
l_4	l_5	l_6	l_7	l_8	l_{11}	l_{12}	l_{13}
5.0 (5.0)	4.8 (4.8)	4.2 (4.2)	3.8 (3.8)	4.95(4.95)	7.0 (7.8)	2.0 (1.6)	1.8 (2.4)
l_{14}	l_{15}	l_{16}	l_{17}	l_{21}	l_{22}	l_{23}	l_{24}
1.0 (1.0)	0.7 (0.7)	3.5 (2.8)	1.0 (1.0)	5.1 (4.2)	1.6 (2.3)	1.1 (1.1)	3.0 (3.2)
l_{31}	l_{32}	l_{33}	l_{34}	l_{35}	l_{36}	s_0	s_1
2.7 (2.7)	1.1 (1.0)	0.7 (0.7)	1.0 (1.0)	2.0 (1.6)	7.0 (7.8)	0.1 (0.1)	0.15 (0.15)
d_x	d_1	d_2	w_s	l_{s1}	R_1, Ω	R_2, Ω	R_3, Ω
1.8 (1.8)	2.35(1.6)	0.8 (1.2)	0.5 (0.5)	5.8 (5.8)	400 (250)	3500 (2000)	1500 (2000)

coupling coefficients of upper bands (M_{12}^H, M_{23}^H) can be further optimised by tuning the value of d_x with constants M_{12}^I and M_{23}^I , based on Fig. 5a.

- vi. Construct the layout of specific DB-FPD. The initial parameters can be calculated based on (4) and (5). Then optimise the return losses of lower passband by tuning the value of l_2 . Also, the return loss in the upper band can be further improved by changing the value of d_x , with almost constant lower passband return losses, based on Fig. 9.
- vii Optimise the isolation performances of the lower band and the upper band by tuning the values of isolation resistors (R_1, R_2 and R_3), and the isolation performance of the upper band can be further adjusted by changing the locations of isolation resistors, based on Fig. 10.
- vii Return step iv until the designed DB-FPD achieves the i. requirements given in step i.

3 Simulated and measured results

To verify the design concept, two DB-FPDs with equal FBW and equal ABW are fabricated on the substrate presented above. The photographs of two designed DB-FPDs are shown in Fig. 11, and the detailed dimensions of two DB-FPDs are given in Table 2.

The measured losses of two SMA connectors operating at 2.45 and 5.80 GHz are 0.25 and 0.60 dB, respectively. Considering the insertion losses of two SMA connectors, the simulated and

measured results of DB-FPD1 and DB-FPD2 are shown in Figs. 12 and 13, respectively. The discrepancy between the measurement and simulation results is due to the inaccuracy of simulation and the error of fabrication as well as measurement. According to Fig. 12a, the measured lower passband bandwidth with return loss better than 15 dB ranges from 2.38 to 2.58 GHz (ABW = 200 MHz, FBW = 8.1%), while the bandwidth of the upper passband ranges from 5.58 to 6.05 GHz (ABW = 470 MHz, FBW = 8.1%). The measured minimum insertion losses in the lower and upper passbands are 3.54 and 3.90 dB, respectively, including the 3 dB power splitting loss. As observed in Fig. 12b, in the wideband responses (DC to 9 GHz), the isolation performance between ports 2 and 3 (S_{23}) is better than 12.0 dB.

According to Fig. 13a, the measured lower passband bandwidth with return loss better than 15 dB ranges from 2.27 to 2.57 GHz (ABW = 300 MHz, FBW = 12.4%), while the bandwidth of upper passband ranges from 5.71 to 6.01 GHz (ABW = 300 MHz, FBW = 5.1%). The measured minimum insertion losses in the lower and upper passbands are 3.60 and 4.00 dB, respectively, including the 3 dB power splitting loss. As observed in Fig. 13b, in the wideband responses (DC to 9 GHz), the isolation performance between ports 2 and 3 (S_{23}) is better than 13.0 dB.

In order to evaluate the passband selectivity performance of the FPDs, the steepness factor (A_s) defined as the ratio of the 3 dB bandwidth to the 30 dB bandwidth, as shown in (9), is introduced [16]. The detailed comparisons of designed DB-FPDs with state-of-the-art published works are provided in Table 3. As observed,

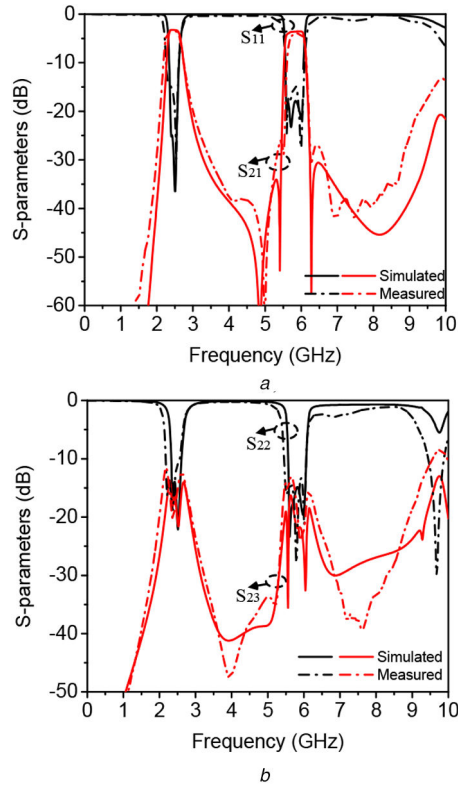


Fig. 12 Simulated and measured results of the fabricated DB-FPD1
 (a) Transmission characteristics, (b) Output return loss and isolation

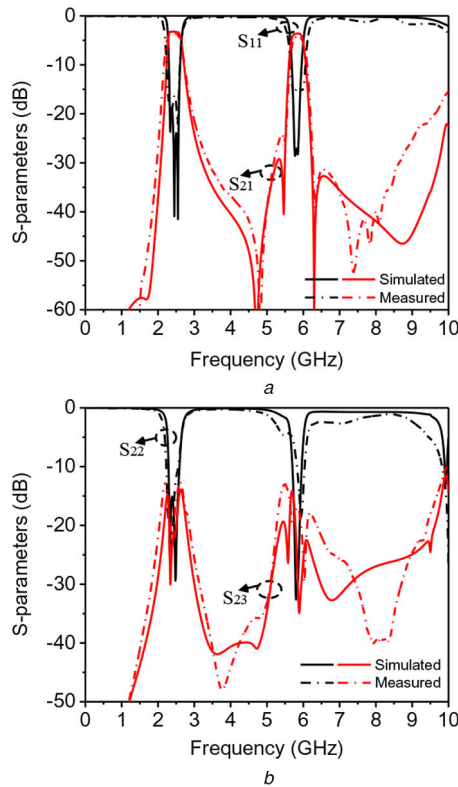


Fig. 13 Simulated and measured results of the fabricated DB-FPD2
 (a) Transmission characteristics, (b) Output return loss and isolation

the proposed DB-FPD structure exhibits compact size, independently controllable passband bandwidths and high-frequency selectivity:

$$\text{Steepness factor } (A_S) = \frac{BW_{3\text{dB}}}{BW_{30\text{dB}}} \quad (9)$$

4 Conclusions

In conclusion, a compact DB-FPD structure with ICBW is presented. The designed DB-FPD structure is composed of four shorted G-shaped resonators, two shorted T-shaped resonators as well as three isolation resistors, and MSLs are etched on shorted patch resonators to introduce resonance in the upper band. The presented DB-FPD structure has the advantages of high-frequency

Table 3 Comparisons between the proposed DB-FPDs and published similar designs

Ref.	Frequency, GHz	FBW ($S_{11} < -15\text{dB}$), %	ABW ($S_{11} < -15\text{dB}$), MHz	IL, dB	Isolation S_{23} , dB	Size $\lambda_g \times \lambda_g$	ICBW	Steepness factor (A_S)
[6]	1.8/3.0	/	/	3.8/3.9	>8/3	0.44×0.50	N	0.21/0.11
[7]	0.9/2.1	22.2/9.5	200/200	3.2/3.4	>10/11	0.26×0.20	N	0.12/0.11
[9]	1.0/1.74	10.0/8.2	100/143	3.9/4.2	>12/12	0.41×0.20	N	0.31/0.56
[10]	3.5/5.0	/	/	3.9/4.9	>8/6	0.27×0.35	N	/
[13]	2.4/3.63	10.1/6.3	242/229	3.8/4.0	>15/15	0.26×0.32	N	0.27/0.32
[14]	1.00/1.95	21/6.7	210/130	—	>20/20	1.04×0.74	Y	/
prototype 1	2.44/5.87	8.1/8.1	198/475	3.6/3.9	>12/13	0.24×0.27	Y	0.27/0.62
prototype 2	2.44/5.85	12.4/5.1	300/300	3.6/4.0	>13/17	0.24×0.27	Y	0.31/0.50

selectivity, good isolation performance, compact size and independently controlled passband bandwidths. The detailed design procedures are given in this paper, which are helpful for DB-FPD practical application.

5 Acknowledgments

This work was supported in part by the National Natural Science Foundations of China (No. 61701041, No. 61671084 and No.61821001), in part by the BUPT Excellent PhD Students Foundation (No. CX2019302), and in part by the China Scholarship Council.

6 References

- [1] Chau, W.M., Hsu, K.W., Tu, W.H.: 'Filter-based Wilkinson power divider', *IEEE Microw. Wirel. Compon. Lett.*, 2014, **24**, (4), pp. 239–241
- [2] Deng, P.H., Dai, L.C.: 'Unequal Wilkinson power dividers with favorable selectivity and high-isolation using coupled-line filter transformers', *IEEE Microw. Wirel. Compon. Lett.*, 2012, **60**, (6), pp. 1520–1529
- [3] Cheong, P., Lai, K., Tam, K.: 'Compact Wilkinson power divider with simultaneous bandpass response and harmonic suppression'. IEEE MTT-S Int. Microwave Symp., Anaheim, CA, USA, 23–28 May 2010, pp. 1588–1591
- [4] Song, K.J., Ren, X., Chen, F.L., *et al.*: 'Compact in-phase power divider integrated filtering response using spiral resonator', *IET Microw. Antennas Propag.*, 2013, **8**, (4), pp. 228–234
- [5] Song, K.J., Xu, B.Q., Guo, S., *et al.*: 'Compact three-way filtering Bagley polygon power divider based on composite right/left-handed transmission lines', *IET Microw. Antennas Propag.*, 2017, **12**, (6), pp. 909–912
- [6] Li, Y.C., Xue, Q., Zhang, X.Y.: 'Single-and dual-band power dividers integrated with bandpass filters', *IEEE Trans. Microw. Theory Tech.*, 2013, **61**, (1), pp. 69–76
- [7] Shao, C., Li, Y., Chen, J.X.: 'Compact dual-band microstrip filtering power divider using T-junction structure and quarter-wavelength SIR', *Electron. Lett.*, 2017, **53**, (6), pp. 434–436
- [8] Feng, W.J., Hong, M.L., Che, W.Q.: 'Dual-band balanced-to-unbalanced filtering power divider by coupled ring resonators', *Electron. Lett.*, 2016, **52**, (22), pp. 1862–1864
- [9] Lu, Y.L., Dai, G.L., Wang, Y., *et al.*: 'Dual-band filtering power divider with capacitor-loaded centrally coupled-line resonators', *IET Microw. Antennas Propag.*, 2017, **11**, (1), pp. 36–41
- [10] Li, Q., Zhang, Y.H., Fan, Y.: 'Dual-band in-phase filtering power dividers integrated with stub-loaded resonators', *IET Microw. Antennas Propag.*, 2014, **9**, (7), pp. 695–699
- [11] Huang, F., Wang, J.S., Hong, J.S., *et al.*: 'A new balanced-to-unbalanced filtering power divider with dual controllable passbands and enhanced in-band common-mode suppression', *IEEE Trans. Microw. Theory Tech.*, 2018, **67**, (2), pp. 695–703
- [12] Zhao, X.L., Gao, L., Xu, J.X., *et al.*: 'High-selectivity dual-band filtering power divider using stub-loaded quarter-wavelength resonator', *J. Electromagn. Waves Appl.*, 2015, **29**, (16), pp. 2216–2223
- [13] Zhang, G., Wang, X.D., Yang, J.Q.: 'Dual-band microstrip filtering power divider based on one single multimode resonator', *IEEE Microw. Wirel. Compon. Lett.*, 2018, **28**, (10), pp. 891–893
- [14] Wu, Y.L., Zhuang, Z., Guan, Y.Y., *et al.*: 'Generalized dual-band unequal filtering power divider with independently controllable bandwidth', *IEEE Trans. Microw. Theory Tech.*, 2017, **65**, (10), pp. 3838–3848
- [15] Hong, J.S.G., Lancaster, M.J.: 'Microstrip filters for RF/microwave applications' (John Wiley & Sons, New York, USA, 2004)
- [16] Williams, A., Taylor, F.J.: 'Electronic filter design handbook' (McGraw-Hill, New York, NY, USA, 2006, 4th edn.)